

Effects of curvature and interactions on the dynamics of the deconfinement phase transition.

Deepak Chandra ¹ and Ashok Goyal ²

Department of Physics and Astrophysics,

University of Delhi, Delhi-110007, India.

and Inter University Center for Astronomy and Astrophysics,

Ganeshkhind, Pune-411007, India.

Abstract

We study the dynamics of first-order confinement-deconfinement phase transition through nucleation of hadronic bubbles in an expanding quark gluon plasma in the context of heavy ion collisions for interacting quark and hadron gas and by incorporating the effects of curvature energy. We find that the interactions reduce the delay in the phase transition whereas the curvature energy has a mixed behavior. In contrast to the case of early Universe phase transition, here lower values of surface tension increase the supercooling and slow down the hadronization process. Higher values of bag pressure tend to speed up the transition. Another interesting feature is the start of the hadronization process as soon as the QGP is created.

1 Introduction

The ongoing and planned experiments involving heavy ion collisions at RHIC, CERN's SPS and at LHC are aimed at studying the behavior of quantum chromodynamics (QCD) at high energies. It is believed that at these high energies [1] (100 GeV/nucleon at RHIC and 3 TeV/nucleon at LHC in the c.m. frame) a hot baryon free plasma of quarks and gluons (QGP) is expected to be created even as at lesser energies, nuclear collisions at Brookhaven's AGS and at SPS show large stopping of the nuclei and hint at the baryon rich matter. The QGP plasma will soon undergo a phase transition to hadronic matter. The phase transition from QGP to hadron resonance gas (HRG) has been extensively studied in the context of the early Universe where the time scale is of the order of $10^{-6} - 10^{-7}$ s [2-4]. Perturbative finite temperature QCD methods along with relativistic transport theory have been used to study the early stages of the nuclear collisions by computer simulations [5,6]. The initial quantitative picture that emerges is that of a QGP fireball of $\sim 150 fm^3$ created at the initial

¹S. G. T. B. Khalsa College, University of Delhi, Delhi-110007, India.

²E-mail: agoyal@duc.ernet.in

temperature of $\sim 300 - 350$ MeV, which is about twice the expected critical temperature T_c . Studies of quark-hadron phase transition in the early Universe, in heavy ion collisions and in high density nuclear matter in the core of compact stars [7] point to the importance of interactions in the two phases. It has been shown that unless hadronic interactions are taken into account, the hadronic phase again becomes thermodynamically the preferred phase at high temperature and that QCD interactions are important in the QGP phase [8] making the critical parameters depend on the interactions. The lattice results also point to the departure of the QGP equation of state (EOS) from the ideal gas EOS even at temperatures well above T_c . However there still remain uncertainties in the equation of state in both the confined and the deconfined phases. It has also been pointed out that in situations in which nucleation takes place, the curvature energy $8\pi\gamma r$, a term in the free energy in addition to the surface energy term $4\pi r^2\sigma$ (where σ and γ are the surface and curvature energy densities respectively) also plays an important role and should be kept in the calculation of the nucleation rate [9-12]. It is in this context that the above experiments will go a long way in establishing the dynamics of the phase transition and the final picture that will emerge would be of great interest in astrophysics and cosmology. If the phase transition from quark gluon plasma to confined hadronic matter is a first order thermodynamic phase transition, the transition would proceed through the nucleation of hadronic bubbles. Conventionally, the QGP would supercool to temperature below T_c only then the nucleation starts. The bubbles greater than the critical size would expand driving the QGP phase into smaller and smaller regions thereby converting more and more matter into the hadronic phase. The expansion of the bubble would be accompanied by the release of latent heat which will reheat the plasma shutting off further nucleation. If the phase transition has to be completed, the latent heat must be gotten rid of. Such studies have been made in the context of the early Universe where it has been shown that phase transition proceeds in the expanding Universe after the Universe supercools to a temperature below T_c , the expanding bubbles then reheat the Universe expelling the QGP phase till the entire Universe is converted to the hadronic phase. The time of completion and the degree of supercooling depends on the EOS and the parameters like the Bag pressure and the surface tension [3].

Csernai and Kapusta [6] have applied a recently computed nucleation rate to a first order phase transition in a set of rate equations to study the time evolution of QGP in heavy ion collisions. Based on Bjorken hydrodynamics and on current parameter values, they find the transition generates about 30 percent extra entropy and also a time delay of $11fm/c$ in completion of the transition. They also estimate that the system should

supercool about 20 percent below T_c before nucleation of hadronic bubbles is rapid enough to start reheating the system. Csernai and Kapusta for the purposes of illustration used noninteracting system of hadrons and QGP. They modelled the hadronic phase by a massless gas of pions and the plasma phase by a gas of gluons and massless quarks of two flavors. In the light of the importance of taking interactions both in the hadronic as well as in the plasma phase for purposes of investigating phase transitions at high energies, temperature and densities as discussed above, we calculate the rate of formation of the hadron bubbles for interacting QGP and hadron resonance gas. It is our endeavour here to examine closely the effects of interactions on the dynamics of phase transition as the hot plasma of quarks and gluons is created and the temperature drops to T_c where a phase mixture of QGP and HRG develops. For this purpose QGP is treated as a gas of massless u, d quarks, massive s quarks and massless gluons. QCD interactions are treated perturbatively to order g^3 and the long range confinement effects are parameterized by the bag pressure B . For the hadron gas we use the known spectrum of low lying baryons and meson resonances and the repulsive interactions between them by incorporating the hard core excluded volume effects. In the literature hadronic interactions have been taken in many different ways (see Ref.7 for example), hadronic interactions can be accounted for through an average mean field repulsive potential arising from the Reid potential and $\pi - \pi$ effective interactions or alternatively, repulsive effects can also be included by modifying the chemical potential as done by Kapusta et al. in a simple method of implementing the mean field theory. One could also use the full fledged framework of relativistic mean field theory itself. It has however been shown by Goyal et al.[7] that in the baryon free case, all the interaction schemes mentioned above give roughly the same value of the hadronic pressure, there are however, marked deviations at very high T and/or at high μ_B regime.

The effect of curvature energy term on the nucleation of hadronic bubbles has been studied earlier [9]. It has been found that it leads to a minima in the free energy in addition to a maxima below the critical temperature and also a minima above T_c , giving rise to spontaneous nucleation of equilibrium sized bubbles. This may contribute to the completion of the phase transition and has interesting consequences. We study here the effect of curvature on the dynamics of the phase transition for several values of the parameters and discuss their consequences.

The plan of the paper is as follows. In section 2 we discuss the bubble nucleation along with the importance of the prefactor which plays a crucial role in guiding the behavior of the nucleation rate. It turns out that the exponential factor is of less relevance here unlike the

case of early Universe where exponent dominates the behavior of the nucleation rate. We also study here the effect of curvature on the nucleation rate and give the two rate equations to study the time evolution of the transition for different parameter values. In section 3 we discuss our result and compare them with the case when interactions and the curvature energy are not present. We also look at the supercooling that takes place and evaluate the behavior of the system with different parameter values. Finally in section 4 we give our conclusions.

2 Bubble nucleation

When the QGP cools through the critical temperature T_c , the new hadron phase becomes preferred. Energetically the new phase remains unfavourable as there is surface free energy associated with the QGP and the hadron gas interface. Creation of bubbles of the new phase are thus unfavourable and all nucleated bubbles with radius less than the critical radius die out but those with radii greater than the critical radius expand until they coalesce with each other. Thus supercooling occurs before the new hadron phase actually appears and takes over. Consequently reheating takes place due to the release of latent heat. The critical radius is obtained by extremizing the thermodynamic work expanded to create a bubble, i.e.

$$W \equiv -\frac{4\pi}{3}r^3(P_h - P_q) + 4\pi r^2\sigma - 8\pi(\gamma_q - \gamma_h)r, \quad (1)$$

where P_h and P_q are the pressures in the hadronic and quark phase respectively, σ is the surface tension and $\gamma = (\gamma_q - \gamma_h)$ is the curvature coefficient and has been estimated in [9]. Following Mardor and Svetitsky the curvature energy in the MIT model for massless quarks is given by

$$E_c = \frac{gr}{3\pi} \int_0^\infty dk k \{1 + \exp(k - \mu_B)/T\}^{-1} \quad (2)$$

where g is the statistical weight and r the radius. We get $\gamma \simeq \gamma_q \equiv \frac{T^2}{16}$, where we have assumed $\gamma_h \ll \gamma_q$ following [11] and μ_B to be negligible compared to T . According to Madsen [10], the assumption of zero strange-quark mass in the curvature term should be relaxed but presently no calculation of the curvature term for massive quarks exists. The surface tension is mainly due to the finite strange quark mass as the massless particles do not contribute to the surface term in the free energy. The critical radius is obtained by putting $\frac{\partial W}{\partial r} = 0$ and we get an extremum below T_c given as

$$r_{c+} = \frac{\sigma}{\Delta P} (1 + \sqrt{1 - \beta}) \quad (3)$$

where $\Delta P = P_h - P_q$ and $\beta = \frac{2\Delta P}{\sigma^2}\gamma$. Since β is positive definite, a real solution exists only if $\beta \leq 1$. This critical radius is actually a maximum. There is another extremum solution (a minima) given by the critical radius

$$r_{c-} = \frac{\sigma}{\Delta P}(1 - \sqrt{1 - \beta}) \quad (4)$$

These bubbles correspond to equilibrium bubbles which stabilise to their critical size r_{c-} and do not grow. The free energies of the critical sized bubbles are given by

$$W_{c+} = \frac{4\pi\sigma^3}{3\Delta P^2}[2 + 2(1 - \beta)^{3/2} - 3\beta] \quad (5)$$

and

$$W_{c-} = \frac{4\pi\sigma^3}{3\Delta P^2}[2 - 2(1 - \beta)^{3/2} - 3\beta] \quad (6)$$

respectively for the two critical radii. β decides the effect of the curvature term and decreases the critical radius for the expanding bubbles. The existence of a critical radius corresponding to the minimum of the free energy is a consequence of the curvature term. In fact there is a extremum in the free energy even above the critical temperature for all starting temperatures of the plasma. This extremum is also a minimum and the corresponding critical radius and the free energy are given by

$$r_{c+>} = \frac{\sigma}{\Delta P}(-1 + \sqrt{1 + \beta}) \quad (7)$$

$$W_{c+>} = \frac{4\pi\sigma^3}{3\Delta P^2}[2 - 2(1 + \beta)^{3/2} + 3\beta] \quad (8)$$

Significantly, the restriction of $\beta \leq 1$ is not present for these bubbles. This feature of the curvature term ensures that the phase transition actually begins well above the critical temperature (as soon as the plasma is formed) by the nucleation of equilibrium sized bubbles of the hadron phase, and this continues till below the critical temperature when the expanding bubbles also join them and start the rapid nucleation and expansion of the hadron phase. As pointed out earlier, below T_c if β becomes greater than one, nucleation of both types of critical bubbles disappear. The phase transition can now take place by the expansion of all the already nucleated critical bubbles r_{c+} , r_{c-} and $r_{c+>}$. This is because the critical radius r_c and the critical free energy W_c necessary for creation of growing bubbles become zero. This essentially means that the phase transition now gets rolling and completes fast. Sooner β becomes greater than 1, faster will this process dominate the phase transition. As we will see, for certain reasonable values of the parameters (B and σ) β becomes greater than 1 almost near T_c causing unrestrained expansion of all the bubbles (ones above T_c as well as whatever exists below it) and completion of the phase transition.

The bubble nucleation rate (number of bubbles formed per unit time per unit volume) at temperature T is given by

$$I = I_0 e^{-W_c/T} \quad (9)$$

where I_0 is the prefactor having dimensions of T^4 . The prefactor used traditionally in the early Universe studies is given by $I_0 = (W_c/2\pi T)^{3/2} T^4$. Csernai and Kapusta [6] have recently calculated this in a coarse grain effective field theoretic approximation to QCD and give

$$I_0 = \frac{16}{3\pi} \left(\frac{\sigma}{3T} \right)^{3/2} \frac{\sigma \eta_q r_c}{\xi_q^4 (\Delta w)^2}$$

where $\eta_q = 14.4T^3$ is the shear viscosity in the plasma phase, ξ_q is a correlation length of order 0.7 fm in the plasma phase, and Δw is the difference in the enthalpy densities of the two phases. This nucleation rate is limited by the ability of dissipative process to carry latent heat away from the bubbles surface as indicated by the dependence on the viscosity. The above expression however gets modified in the present case because of the presence of the equilibrium bubbles. We now have different I 's depending on which kind of bubbles are being discussed, namely I_+ , I_- and $I_{+>}$ corresponding to critical radii r_{c+} , r_{c-} and $r_{c+>}$ respectively.

The pressure in the QGP phase can be calculated by using the thermodynamic potential given in Kapusta and Shuryak [7]. For the hadron phase we use the known masses of the low lying 33 baryons and 45 mesons whose masses and degeneracy factors are taken from the Particle Data Group Summary [13]. The hadronic pressure and number densities for non-interacting point baryons and mesons are given by the usual thermodynamic relations. One of the simplest ways to account for the short range repulsive forces as discussed above is by considering the finite volume of the baryons that modify the space available for occupation in a manner akin to that of a Van der Waal's equation. We take baryons and antibaryons to have the same size as protons, given by $V_p = m_p/4B$ where B is the bag pressure. A radius r_p lying between 0.6 fm and 0.8 fm is often used [7]. The hadronic pressure and baryon densities corrected for finite volume effects are now given by

$$P_h = \frac{\sum_b P_b^{pt}}{1 + \sum_b n_b^{pt} V_p} + \frac{\sum_{\bar{b}} P_{\bar{b}}^{pt}}{1 + \sum_{\bar{b}} n_{\bar{b}}^{pt} V_p} + \sum_m P_m^{pt} \quad (10)$$

$$n_B = \frac{\sum_b n_b^{pt}}{1 + \sum_b n_b^{pt} V_p} + \frac{\sum_{\bar{b}} n_{\bar{b}}^{pt}}{1 + \sum_{\bar{b}} n_{\bar{b}}^{pt} V_p} \quad (11)$$

where b , \bar{b} and m stand for baryons, anti-baryons and mesons respectively. The pressure equilibrium between the two phases sets T_c which is decided by the parameters in the theory,

essentially by the parameters B and σ . With nucleation rate given by eq.(9), one would like to know the fraction of space $h(t)$ which is in the hadronic phase at the given time t as measured in a local comoving frame of the expanding system. Guth and Weinberg [14] have proposed a formula for $h(t)$ in the cosmological first order phase transition. Csernai and Kapusta [6] have given a more accurate kinetic equation than the one used by Guth and Weinberg and it allows for the transition to complete. If the system cools to T_c at time t_c , then at some later time t , the fraction of space which has been converted to hadronic gas is given by them as

$$h(t) = \int_{t_c}^t dt' I(T(t')) \{1 - h(t')\} V(t', t) \quad (12)$$

where $V(t, t')$ is the volume of a bubble at time t which had been nucleated at the earlier time t' ; taking bubble growth into account. Here we have neglected bubble collisions and fusion. The above expression however gets modified in the present case because of the presence of the equilibrium bubbles. Now we have an additional contribution to the hadron fraction from the bubbles that are nucleated above the critical temperature plus those that are nucleated below the critical temperature and do not grow in size (unless $\beta > 1$). So, the new expression is now given by

$$\begin{aligned} h(t) = & \int_{t_c}^t dt' I_+(T(t')) \{1 - h(t')\} V(t', t) \\ & + \int_{t_c}^t dt' I_-(T(t')) \{1 - h(t')\} \frac{4\pi}{3} r_{c-}^3(T(t')) \\ & + \int_{t_0}^{t_c} dt' I_{+>}(T(t')) \{1 - h(t')\} \frac{4\pi}{3} r_{c+>}^3(T(t')) \end{aligned} \quad (13)$$

The dynamical equation which couples time evolution of temperature to $h(t)$ is obtained by using the longitudinal scaling hydrodynamics of Bjorken. It is given by

$$\frac{de}{dt} = -\frac{w}{t} \quad (14)$$

where $e(T)$ and $w(T)$ are the energy and enthalpy densities respectively being given by $e(T) = h(t)e_h(t) + (1 - h(t))e_q(t)$, e_h and e_q being the hadron and quark energy densities at time t respectively, likewise for the enthalpy density. Following [16] the growth velocity of bubbles is taken to be $v(T) = v_0(1 - T/T_c)^{3/2}$ where $v_0 = 3c$ for $T > 2/3T_c$. This gives $v < c/\sqrt{3}$, the speed of sound for a massless gas. We have assumed that if supercooling takes T below $2/3T_c$ then v is given by $c/\sqrt{3}$. This ensures that closer T is to T_c slower the bubbles grow. The volume of an expanding bubble at time t is then given by

$$V(t', t) = \frac{4\pi}{3} \{r_{c+}(T(t')) + \int_{t'}^t dt'' v(T(t''))\}^3 \quad (15)$$

In calculations we use the parameters $\xi_q = 0.7 fm$ and $\eta_q = 14.4T^3$ as in [6]. σ and B are varied to study the behavior of the phase transition as the QGP cools and hadron bubbles are formed. We solve the two coupled equations (13) and (14) for different values of the parameters B and σ . The nucleation time is defined as

$$\tau^{-1} = \frac{4\pi}{3} r_c^3 I$$

neglecting bubble growth. In our case we have a contribution to τ from I_+ , I_- below T_c and $I_{+>}$ above T_c .

3 Results and Discussion

We find that the inclusion of the interactions in both the plasma phase and the hadron gas phase lowers the critical temperature, so higher values of the bag pressure are required for having reasonable values of T_c . For example, the value $B^{1/4} = 300 MeV$ gives a $T_c \sim 188 MeV$ whereas $B^{1/4} = 235 MeV$ gives a $T_c \sim 144 MeV$. We show below plots of free energy vs radius of a hadron bubble, nucleation time vs temperature, temperature vs time and hadron fraction vs time etc. In fig.1 we plot the free energy of a hadron bubble against it's radius in the QGP plasma. For temperatures just above the critical temperature we see that the effect of the curvature term is to produce a minima in the free energy which is to be contrasted with no extremum without a curvature term. Fig.1a pertains to $T = 1.01T_c$ and the dashed and the dotted curves are without the curvature term. It is clearly seen that equilibrium sized hadron bubbles appear even above the critical temperature (solid and long dashed curves). Fig.1b is plotted for a different set of parameters. The lower panel is plotted just below the critical temperature at $T = 0.99T_c$. Here we find that below the critical temperature the curvature effect produces a minima as well as a maxima in the free energy. The maxima bubbles grow whereas the minima bubbles reach an equilibrium size. The dashed and the dotted curves are without the curvature effect showing the presence of only the maximum sized bubbles. Figures 1c and 1d plot the same curves but for a different set of the parameters. It is interesting to note that for $B^{1/4} = 300 MeV$, $\sigma \sim 7 MeV/fm^2$ ($\sigma^{1/3} = 65 MeV$) and $T = 0.99T_c$ the free energy has no extremums, only a maximum value at zero (long dashed), indicating that critical radius is zero and all existing bubbles can now expand to reduce the free energy. In such cases β becomes greater than 1 soon after T_c is crossed and there cannot be nucleation of any fresh bubbles. The expansion of all the existing bubbles ensures completion of the transition. In Fig.2 we have shown the plot of T/T_c against time. The temperature of the QGP plasma decreases with time till T_c , when the

phase transition conventionally begins and supercooling starts. The degree of supercooling depends on the parameters and can be a significant fraction of T_c . The important feature to see here is that the prefactor I_0 is the deciding factor for supercooling and the duration of the transition rather than the exponent. On the other hand in the early Universe studies, it is the exponent which decides the behavior of the transition. In fig.2a the dashed curve (without curvature) and the solid curve (with curvature) are for parameters $B^{1/4} = 235 \text{ MeV}$ and $\sigma = 50 \text{ MeV}/\text{fm}^2$ ($\sigma^{1/3} \sim 125 \text{ MeV}$). As can be seen they overlap, indicating that in this case the curvature term does not make any difference. This value of the surface tension is rather large and in fact exceeds the upper limit set in [15]. However, for the parameters $B^{1/4} = 235 \text{ MeV}$ and $\sigma = 20 \text{ MeV}/\text{fm}^2$ ($\sigma^{1/3} \sim 92 \text{ MeV}$) there is a delay in the completion of the phase transition when the γ term is included (long dashed) compared to the no γ (dotted) case. The delay is of the order of 13 fm and is because of β becoming greater than one a little below T_c with consequent stoppage of all bubble nucleation. When the γ term is not taken, there is no such stoppage and continuous nucleation ensures faster completion. Figure 2b shows the same curves for the parameters $B^{1/4} = 235 \text{ MeV}$, $\sigma \sim 7 \text{ MeV}/\text{fm}^2$ and $B^{1/4} = 300 \text{ MeV}$, $\sigma \sim 7 \text{ MeV}/\text{fm}^2$. In the latter case, the curvature term completely inhibits bubble nucleation below T_c and only the equilibrium bubbles formed above T_c expand to complete the phase transition (long dashed). This corresponds to the case of no extremum in free energy (fig.2b). The inclusion of γ term in this case actually reduces the time to complete the phase transition. This can be contrasted with the case corresponding to the other set of parameters in fig.1d and the cases shown in fig.2a. Comparing with the no curvature case, It is seen that increasing B speeds up the phase transition whereas decreasing it slows it down if the γ term is included. We also see that the decrease in the surface tension increases the supercooling of the plasma by significant amount (can be close to 50 percent). However, increasing B reduces supercooling when γ is included.

Next we look at the nucleation rate vs T/T_c . One can see from these graphs (figures 3a and 3b) that nucleation of hadronic bubbles can start even above the critical temperature when we include the curvature energy. The effect of decreasing σ is to suppress nucleation. We may note that in the early Universe reverse is the case, and it happens because there the exponent drives the nucleation rate whereas in QGP the prefactor drives the nucleation. The point at which β becomes greater than one is clearly visible when curvature term is included. In figure 3a the long dashed curve terminates at the point where further nucleation stops. It is also clear that nucleation starts the moment the plasma is created well above the critical temperature if the curvature term is included. Figure 3b shows that for smaller surface

tension the β term becomes greater than one soon after crossing through T_c (solid and the long dashed curves). The other two curves shown are without the curvature terms and so begin below the critical temperature.

In figure 4 upper panel the critical radius of a bubble is plotted as a function of T/T_c for those bubbles which are nucleated at the minima in the free energy. These bubbles in general are nucleated above $T_c(r_{c+})$ as well as below $T_c(r_{c-})$. In fig.4a we see that for the parameters $B^{1/4} = 235\text{MeV}$, $\sigma = 20\text{MeV}/\text{fm}^2$ the bubbles keep nucleating from above the critical temperature to well below it. However for another set ($B^{1/4} = 300\text{MeV}$, $\sigma \sim 7\text{MeV}/\text{fm}^2$) these bubbles are no longer nucleated soon after crossing T_c . In figure 4b we find this feature in both the parameter sets. In all such situations (where β becomes greater than 1) the completion of the phase transition is ensured by expansion of already nucleated bubbles. The lower panel plots the critical bubble radius r_{c+} corresponding to the maxima in the free energy as a function of T/T_c for temperatures below the critical temperature ($T < T_c$). We see in both the graphs 4c and 4d that the critical radius goes down with temperature. In figure 4c we see that the critical bubble radius goes to zero when $\beta > 1$ (long dashed curve having $\gamma \neq 0$). If no curvature term is present then the critical size does not go to zero. Even with curvature term, large σ does not allow critical radius to go to zero (solid curve). Figure 4d plotted for a different set of parameters has similar features except that for $B^{1/4} = 300\text{MeV}$, $\sigma \sim 7\text{MeV}/\text{fm}^2$ the critical radius below T_c is zero. The only bubbles that can expand are the ones already nucleated above T_c .

Finally, figures 5a and 5b show the hadron fraction h as a function of time t as the phase transition proceeds to its completion. Figure 5a shows the overlap for one parameter set given there (solid and dashed curves) and clearly shows that if we decrease the surface tension the phase transition proceeds slowly (long dashed curve) unlike the case in early Universe studies. The effect of γ has a mixed behavior depending on the value of the bag pressure. Figure 5b shows that for low bag pressures, the effect of γ is to delay the phase transition (solid curve) but for larger values of B we see that the curvature correction actually speeds up the process of hadronization (long dashed curve).

The idealized Maxwell construction with the correction to the QGP as well as the hadron gas that we have studied here shows that the time range of the phase transition is actually less than what has been given in [6]. For the same parameter values as given in [6] we find that in the ideal case with corrections, the phase transition ranges from 2.5 fm to 22 fm whereas without the corrections it ranges from 3 fm to 37 fm. If we compare our study with this corrected ideal Maxwell construction, we find that for $B^{1/4} = 235\text{MeV}$ the

presence of the curvature term delays the transition to 31 fm for $\sigma = 50 \text{ MeV fm}^{-2}$, to 53 fm for $\sigma = 20 \text{ MeV fm}^{-2}$ and to more than 60 fm for $\sigma \sim 7 \text{ MeV fm}^{-2}$. For $B^{1/4} = 300 \text{ MeV}$ the ideal case stretches from 1.9 fm to 6.8 fm but curvature introduces a delay and the transition extends to 12 fm for $\sigma = 50 \text{ MeV fm}^{-2}$, to 16 fm for $\sigma = 20 \text{ MeV fm}^{-2}$ and to 27 fm for $\sigma \sim 7 \text{ MeV fm}^{-2}$. It is interesting to note that the ideal Maxwell case range is 1.5 fm to 2.8 fm for $B^{1/4} = 350 \text{ MeV}$, but $\sigma \sim 7 \text{ MeV fm}^{-2}$ with the curvature term produces a range from 1.5 fm to 16 fm.

4 Conclusions

In conclusion, we have presented in detail the mechanism of the phase transition of the QGP fireball from its creation to its subsequent hadronization in an ultrarelativistic nuclear collision. The inclusion of the interactions in both phases along with the curvature energy term introduces subtleties that are both interesting and quantitative in nature. Broadly, we can summarize that whereas interactions lower the critical temperature, the combined effect of interaction and curvature energy is to affect both the degree of supercooling and the extent of the delay in the phase transition. Smaller values of the surface tension can enhance supercooling to almost 50 percent and also increase the delay in the hadronization process whereas larger values of the bag pressures speed up the hadronization process. $\sigma^{1/3} = 65 \text{ MeV}$ ($\sigma \sim 7 \text{ MeV fm}^{-2}$) is a reasonable value according to the literature and anything above $\sigma^{1/3} = 105 \text{ MeV}$ ($\sigma \sim 30 \text{ MeV fm}^{-2}$) seems to be on the higher side [15]. The critical temperature is decided by the bag pressure and the inclusion of interactions in the two phases suppresses it. $T_c \sim 170 - 180 \text{ MeV}$ is favored in the literature, so a bag pressure in excess of 300 MeV seems to be on the higher side. Inclusion of the curvature effect has a mixed behavior in that, for larger values of B the transition is speeded up whereas for smaller values of B delay is enhanced. Another interesting observation is that the hadronization actually begins the moment the QGP is created, through equilibrium sized bubbles and is later joined by the expanding bubbles below the critical temperature. For reasonable parameter values the nucleation of bubbles below T_c can get stopped when $\beta > 1$ and now even the equilibrium sized bubbles join the expansion to complete the phase transition. Finally, for the ideal Maxwell construction, inclusion of interactions reduces the range of the transition but the presence of the curvature term introduces a delay in the completion of the transition compared to the ideal case.

Acknowledgements

This work was partially supported under the SERC Scheme of The Department of Science and Technology (DST), India. One of us (A.G.) is thankful to U.G.C. for partial financial support.

Figure Captions

Fig. 1. Free energy W in units of MeV as a function of bubble radius r in fm. In fig.1a Solid (with γ) and dashed (without γ) curves are for $B^{1/4} = 235\text{MeV}$ and $\sigma = 50\text{MeVfm}^{-2}$. Long dashed (with γ) and dotted (without γ) curves are for $B^{1/4} = 235\text{MeV}$ and $\sigma = 20\text{MeVfm}^{-2}$. In fig.1b Solid (with γ) and dashed (without γ) curves are for $B^{1/4} = 235\text{MeV}$ and $\sigma \sim 7\text{MeVfm}^{-2}$. Long dashed (with γ) and dotted (without γ) curves are for $B^{1/4} = 300\text{MeV}$ and $\sigma \sim 7\text{MeVfm}^{-2}$. Both the curves 1a and 1b are at a temperature of $1.01T_c$. In the lower panel the curves 1c and 1d are labelled as in Fig.1a and 1b respectively except that both are at a temperature of $.99T_c$.

Fig. 2. Temperature T/T_c as a function of time t in fm. In fig.2a and 2b Solid, dashed, dotted and long dashed curves are labelled as in fig. 1a and 1b respectively.

Fig. 3. Log of the nucleation time τ (Tau) in units of fm/c as a function of temperature. The figures 3a and 3b are labelled as in fig.1a and 1b respectively.

Fig. 4. Upper panel shows critical bubble radius r_c in fm as a function of T/T_c . They are the minimum free energy equilibrium critical bubbles. The solid and long dashed curves are both with γ correction. These bubbles do not exist without the curvature correction. Figures 4a and 4b are labelled as in fig.1a and 1b respectively. Lower panel shows critical bubble radius r_c in fm as a function of T/T_c . They are the maximum free energy expanding critical bubbles. Figures 4c and 4d are labelled as in fig.1a and 1b respectively.

Fig. 5. The hadron fraction h as a function of time t in fm. Curves in fig.5a and 5b are labelled as in fig. 1a and 1b respectively.

References

- [1] J. D. Bjorken, Phys. Rev. **D27**, 140 (1983)
- [2] C.J. Hogan, Phys. Lett. **B133**, 172 (1983); K. Kajantie and M. Kurki-Suonio, Phys. Rev. **D34**, 1719 (1996); G.M. Fuller, G.J. Mathews and C.R. Alcock, Phys. Rev. **D37**,

- 1380 (1988).
- [3] D. Chandra and A. Goyal, Phys. Rev. **D62**, 063505 (2000).
 - [4] E. Witten, Phys. Rev. **D30**, 272 (1984); A. Applegate and C.J. Hogan, Phys. Rev. **D31**, 3037 (1985); E. Farhi and R.L. Jaffe, Phys. Rev. **D30**, 2379 (1984).
 - [5] K. Geiger and B. Muller, Nucl. Phys. **B369**, 600 (1992).
 - [6] L.P. Csernai and J.I. Kapusta, Phys. Rev. Lett. **69**, 737 (1992); Phys. Rev. **D46**, 1379 (1992) and the references cited therein.
 - [7] J. I. Kapusta, Nucl. Phys. **B148**, 461 (1979); E. V. Shuryak, Phys. Rep. **61**, 71 (1979); J. Cleymans and E. Suhonen, Z. Phys. **C37**, 51 (1987); H. Kuono and F. Z. Takagi, Z. Phys. **C42**, 209 (1989); J. I. Kapusta and K. A. Olive, Nucl. Phys. **A408** 478 (1983); J. D. Walecka, Ann. Phys. NY. **83** 491 (1974); B. D. Serot and J. D. Walecka, Adv. Nucl. Phys. **16** (1986); B. A. Campbell et. al., Nucl. Phys. **B345**, 57 (1990); R. Venugopalan and M. Prakash, Nucl. Phys. **A546**, 718 (1992); J. I. Kapusta et. al., Phys. Rev. **C51**, 901 (1995); N. K. Glendenning, ApJ, **293**, 470 (1985); A. Goyal et. al., ApJ, **452**, 501 (1995).
 - [8] C. P. Singh, Phys. Rev. **D49**, 4023 (1994).
 - [9] I. Mardor and B. Svetitsky, Phys. Rev. **D44**, 878 (1991).
 - [10] J. Madsen, Phys. Rev. Lett. **70**, 391 (1993).
 - [11] J. E. Horvath, Phys. Rev. **D49**, 5590 (1994).
 - [12] A. Goyal and D. Chandra, Astron. Astrophys. **330**, 10 (1998).
 - [13] Particle Data Group, Phys. Rev. **D50**, (1994)
 - [14] A.H. Guth and E.J. Weinberg, Phys. Rev. **D23**, 376 (1981).
 - [15] M. S. Berger and R. L. Jaffe, Phys. Rev. **C35**, 213 (1987).
 - [16] J. C. Miller and O. Pantano, Phys. Rev. **D40**, 1789 (1989); **40**, 3334 (1990).

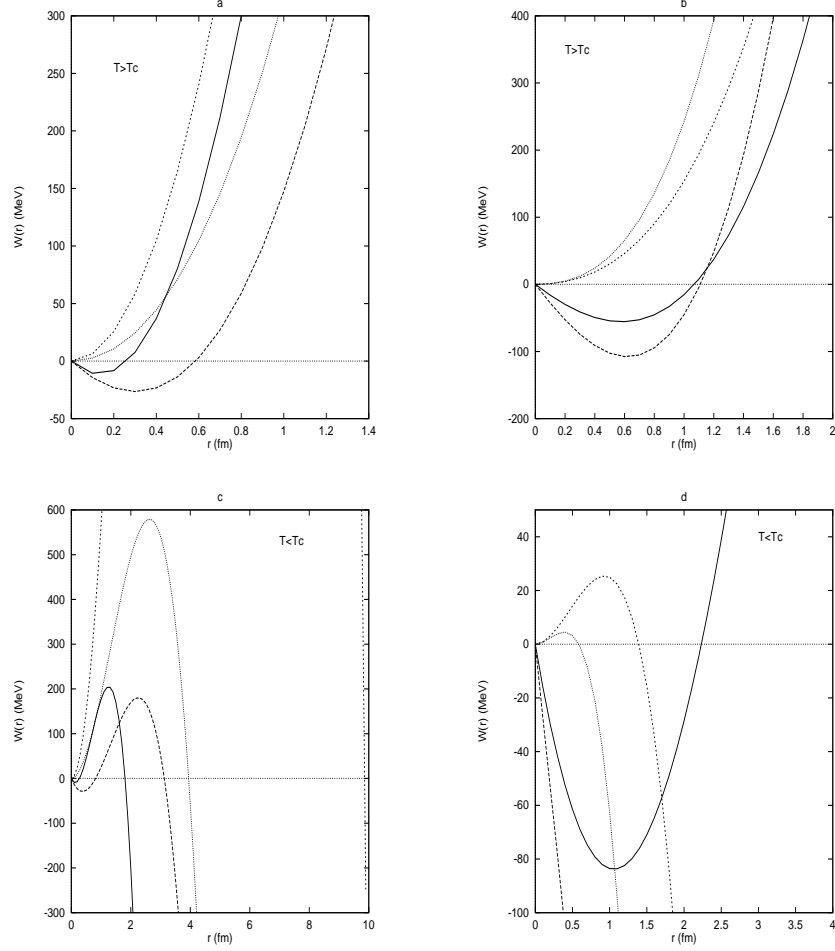


Figure 1: Free energy W in units of MeV as a function of bubble radius r in fm. In fig.1a Solid (with γ) and dashed (without γ) curves are for $B^{1/4} = 235 \text{ MeV}$ and $\sigma = 50 \text{ MeV fm}^{-2}$. Long dashed (with γ) and dotted (without γ) curves are for $B^{1/4} = 235 \text{ MeV}$ and $\sigma = 20 \text{ MeV fm}^{-2}$. In fig.1b Solid (with γ) and dashed (without γ) curves are for $B^{1/4} = 235 \text{ MeV}$ and $\sigma \sim 7 \text{ MeV fm}^{-2}$. Long dashed (with γ) and dotted (without γ) curves are for $B^{1/4} = 300 \text{ MeV}$ and $\sigma \sim 7 \text{ MeV fm}^{-2}$. Both the curves 1a and 1b are at a temperature of $1.01 T_c$. In the lower panel the curves 1c and 1d are labelled as in Fig.1a and 1b respectively except that both are at a temperature of $.99 T_c$.

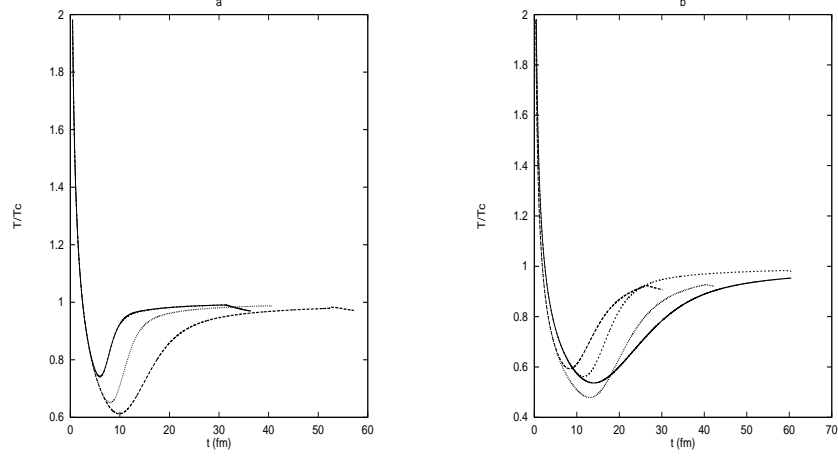


Figure 2: Temperature T/T_c as a function of time t in fm. In fig.2a and 2b Solid, dashed, dotted and long dashed curves are labelled as in fig. 1a and 1b respectively.

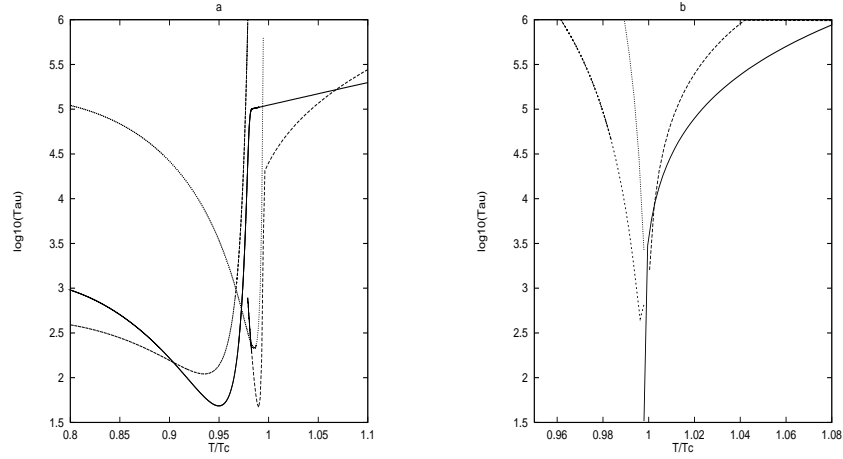


Figure 3: Log of the nucleation time $\tau(\text{Tau})$ in units of fm/c as a function of temperature. The figures 3a and 3b are labelled as in fig.1a and 1b respectively.

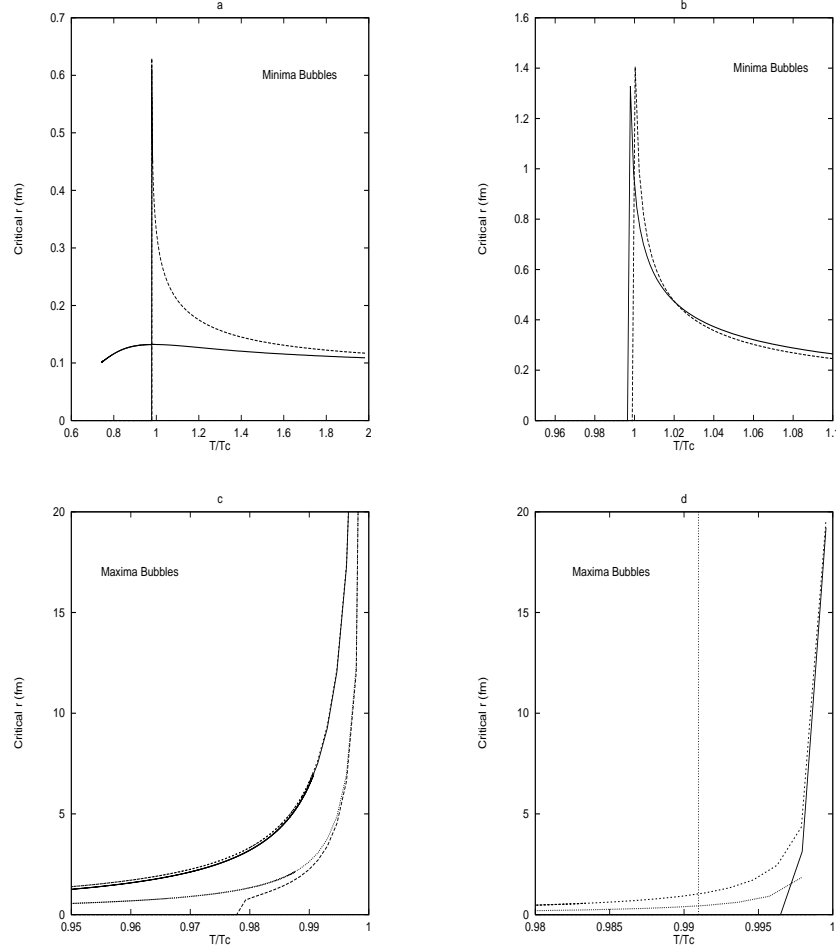


Figure 4: Upper panel shows critical bubble radius r_c in fm as a function of T/T_c . They are the minimum free energy equilibrium critical bubbles. The solid and long dashed curves are both with γ correction. These bubbles do not exist without the curvature correction. Figures 4a and 4b are labelled as in fig.1a and 1b respectively. Lower panel shows critical bubble radius r_c in fm as a function of T/T_c . They are the maximum free energy expanding critical bubbles. Figures 4c and 4d are labelled as in fig.1a and 1b respectively.

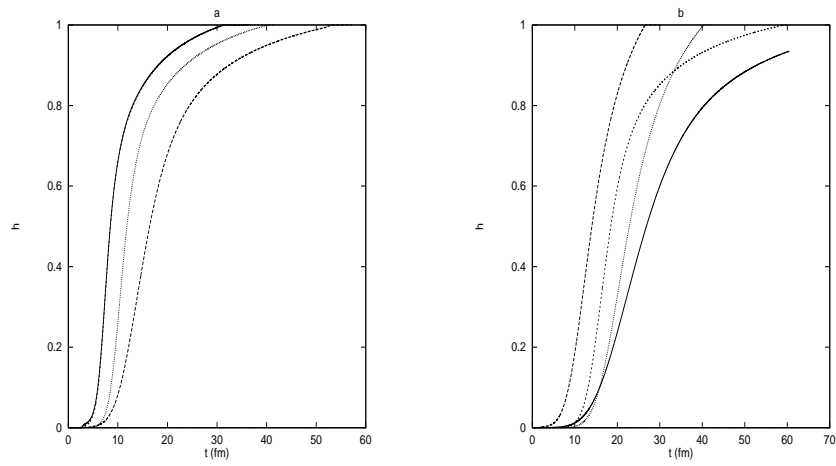


Figure 5: The hadron fraction h as a function of time t in fm. Curves in fig.5a and 5b are labelled as in fig. 1a and 1b respectively.